

# PhaForce: Phase-Scheduled Visual–Force Policy Learning with Slow Planning and Fast Correction for Contact-Rich Manipulation

Mingxin Wang, Zhirun Yue, Renhao Lu, Yizhe Li, Zihan Wang,  
Guoping Pan, Kangkang Dong, Jun Cheng, Yi Cheng, Houde Liu\*

**Abstract**—Contact-rich manipulation requires not only vision-dominant task semantics but also closed-loop reactions to force/torque (F/T) transients. Yet, generative visuomotor policies are typically constrained to low-frequency updates due to inference latency and action chunking, underutilizing F/T for control-rate feedback. Furthermore, existing force-aware methods often inject force continuously and indiscriminately, lacking an explicit mechanism to schedule *when / how much / where* to apply force across different task phases. We propose PhaForce, a phase-scheduled visual–force policy that coordinates low-rate chunk-level planning and high-rate residual correction via a unified *contact/phase* schedule. PhaForce comprises (i) a contact-aware phase predictor (CAP) that estimates contact probability and phase belief, (ii) a Slow diffusion planner that performs dual-gated visual–force fusion with *orthogonal residual injection* to preserve vision semantics while conditioning on force, and (iii) a Fast corrector that applies *control-rate* phase-routed residuals in interpretable corrective subspaces for within-chunk micro-adjustments. Across multiple real-robot contact-rich tasks, PhaForce achieves an average success rate of 86% (+40 pp over baselines), while also substantially improving contact quality by regulating interaction forces and exhibiting robust adaptability to OOD geometric shifts.

## I. INTRODUCTION

Diffusion-based visuomotor policies [1] and recent VLA models [2]–[4] have achieved strong performance on vision-dominant manipulation tasks such as pick-and-place, rearrangement, and folding [5], [6]. However, many real-world skills are inherently *contact-rich*: success depends not only on geometric alignment but also on interaction dynamics such as friction, jamming, and transient impacts [7]–[12]. In such scenarios, vision is often ambiguous or occluded, and critical signals emerge as short-horizon 6D force/torque (F/T) events. For instance, in insertion, being fully seated versus being jammed on the rim can be visually indistinguishable at millimeter scale, while wrench transients reveal misalignment and recovery cues [13]. Similarly, in wiping, visual observations rarely reveal whether the tool is slightly detached or over-pressed [11].

This motivates incorporating F/T (wrench) sensing as physical feedback for contact-rich manipulation. Most force-aware policies encode a short F/T history and fuse it with vision (e.g., concatenation or attention), then use the fused multimodal representation in a chunked generative policy [14]–[17].

However, a key structural mismatch remains underexplored (**Gap-1: timescale mismatch of force feedback**): F/T is a feedback signal whose value lies in rapid closed-loop correction, while generative policies are typically constrained to low-frequency updates by inference latency and action

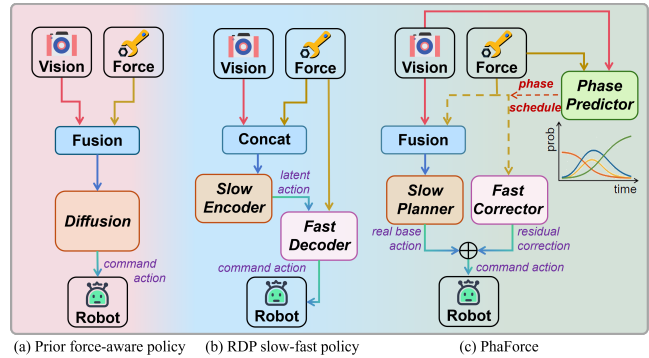


Fig. 1. Comparison of three force-aware policy architectures. Prior works fuse vision and force into a single generative policy, while RDP adopts a slow–fast decomposition without explicit phase scheduling. **PhaForce** introduces an explicit contact/phase schedule to coordinate force usage for both chunk-level planning (Slow) and within-chunk correction (Fast).

chunking. When force is primarily consumed at the action-chunk update rate, short-horizon interaction transients (e.g., stick-slip, micro-impacts, early jamming) can be under-reacted. This calls for an explicit closed-loop correction layer that reacts to force feedback within an action chunk.

Reactive Diffusion Policy [18] takes an important step towards slow–fast execution by coupling chunk-level generative planning with within-chunk reactivity. However, such reactive designs remain largely *phase-agnostic*, often applying high-frequency corrections without explicitly distinguishing which motion channels should be corrected at different stages. Contact-rich manipulation is inherently multi-phase: different stages (e.g., planar search versus normal insertion) demand orthogonal or even mutually exclusive corrective subspaces. Without an explicit phase schedule, high-rate reactivity can introduce spurious corrections in irrelevant subspaces, degrading alignment and potentially leading to jamming behaviors. Prior work therefore lacks an explicit phase schedule to dynamically route force feedback—leaving a critical gap in deciding *when* to trust force, *how much* to use it, and critically, *where* (in which corrective subspace) to apply it (**Gap-2: explicit phase scheduling**) [19], [20].

In this work, we propose **PhaForce**, a *phase-scheduled* slow–fast policy that uses an explicit contact probability and a task-defined phase-belief distribution to coordinate force usage for both chunk-level planning and within-chunk closed-loop correction. Fig. 1 provides an intuitive comparison of three force-aware policy architectures. PhaForce consists of three components: (1) a *contact-aware phase*

*predictor* that outputs a continuous contact probability and a soft distribution over phases, providing an explicit semantic schedule signal; (2) a **Slow** diffusion planner that performs *dual-gated* visual–force fusion for long-horizon action-chunk generation, where contact gates the overall force injection and phase belief modulates the fused representation to maintain vision-dominant semantics via *orthogonal residual injection*; and (3) a **Fast** residual corrector that applies control-rate corrections in *phase-routed* corrective subspaces, trained with physically motivated supervision constructed from the *virtual target pose*. The final control command is obtained by composing the **Slow** real base action with the **Fast** residual correction.

Our contributions are summarized as follows:

- We propose **PhaForce**, a *phase-scheduled* slow–fast policy that unifies force-aware chunk-level generative planning with control-rate residual correction.
- We introduce an explicit scheduling signal (contact probability + phase belief) that decides *when / how much* to use force for planning and *where* to correct during execution, realized by dual-gated fusion with orthogonal residual injection in **Slow** and phase-routed corrective subspaces in **Fast**.
- We validate PhaForce on multiple real-robot contact-rich manipulation tasks, showing consistent improvements over strong baselines in both ID and OOD settings.

## II. RELATED WORK

### A. Force-Aware Visuomotor Policy Learning

A prevalent paradigm for force-aware imitation learning encodes a short history window of 6D wrench measurements and fuses the resulting force representation with visual features—typically via feature concatenation [14], [17], [21], [22] or attention-based cross-modal interaction [15], [23]–[27], treating the multimodal feature as the observation for a visuomotor policy. FoAR [19] modulates force usage with a predicted future contact probability to suppress noisy wrench signals in free-space and amplify force under contact. ForceVLA [16] employs a force-aware Mixture-of-Experts block, where expert routing varies with task progress and can implicitly specialize across interaction stages.

Beyond fusion, Stepputtis et al. [8] introduce a continuous phase variable (from 0 to 1) to represent task progress and feed it to skill primitives for contact-rich manipulation. TA-VLA [13] highlights torque transients as reliable event signals that reveal contact outcomes and naturally support intent switching (e.g., detect failure and retry).

However, existing approaches still lack an explicit, task-defined *probabilistic phase belief* mechanism to interpretably schedule *when / how much* force should be fused with vision and to exploit force cues without degrading visual task semantics.

### B. Slow–Fast Policy Learning under Action Chunking

Despite recent progress in force-aware visuomotor policy learning, many methods still rely on action-chunk generation,

resulting in near open-loop execution within each chunk and delaying the use of wrench transients that often signal contact anomalies and intent switches. ManipForce [20] introduces frequency-aware multimodal representations, but still follows the chunked diffusion paradigm without dedicated within-chunk force-driven correction.

Reactive Diffusion Policy [18] adopts a slow–fast architecture, where a slow diffusion model predicts low-rate latent action chunks and a fast decoder leverages high-rate wrench feedback to autoregressively generate fine-grained control commands within each chunk. Subsequent analyses [28] suggest that latent chunk compression may reduce free-space motion precision and degrade millimeter-level approach/contact localization. More broadly, wrench feedback in existing designs is still primarily used for within-chunk local refinement, leaving open a structured, task-semantic mechanism for long-horizon intent switching and phase-dependent correction. ImplicitRDP [28] further explores end-to-end structural slow–fast learning, yet explicit and interpretable phase-level scheduling remains underexplored.

Overall, it remains underexplored how to close the loop at high control rates while coordinating long-horizon planning and residual correction in an interpretable, phase-dependent manner.

## III. METHOD

In this section, we present **PhaForce**, a phase-scheduled visual–force policy for contact-rich manipulation (Fig. 2). We first formalize the problem and specify the slow–fast execution pipeline under action chunking (Sec. III-A). We then introduce a *contact-aware phase predictor* that outputs a continuous contact probability and a phase-belief distribution (Sec. III-B). Finally, we describe how this phase belief coordinates both low-frequency task-intent planning in the **Slow** planner (Sec. III-C) and high-frequency residual correction in the **Fast** corrector (Sec. III-D).

### A. Problem Formulation and Preliminaries

**Observation inputs.** At each timestep  $t$ , we define two observation views tailored to slow–fast execution. The *planner observation*  $o_t^p = (\mathcal{I}_t, w_t^{\text{hist}}, s_t)$  includes multi-view RGB images  $\mathcal{I}_t$ , wrench history  $w_t^{\text{hist}}$  expressed in the TCP frame, and proprioception  $s_t$ . The *corrector observation*  $o_t^c = (w_t^{\text{hist}}, s_t)$  excludes images and uses only low-dimensional signals. Here we define  $H_w$  as the wrench-history window length, capturing short-term interaction dynamics.

**Policy outputs.** We learn a slow–fast policy pair  $(\pi_{\text{slow}}, \pi_{\text{fast}})$  under action chunking with two update rates. As shown in Fig. 2(c),  $f_c$  denotes the *control frequency* at which the robot is commanded and the **Fast** corrector is evaluated, and  $f_s$  denotes the *inference frequency* of the **Slow** planner, typically  $f_s \ll f_c$  due to inference latency.  $\pi_{\text{slow}}$  predicts a nominal action chunk; we denote by  $T_t^{\text{slow}} \in SE(3)$  the corresponding nominal TCP pose at control step  $t$ . In contrast,  $\pi_{\text{fast}}$  consumes  $o_t^c$  at  $f_c$  and predicts a small delta pose  $\Delta T_t^{\text{fast}} \in SE(3)$  in the TCP frame for high-rate residual

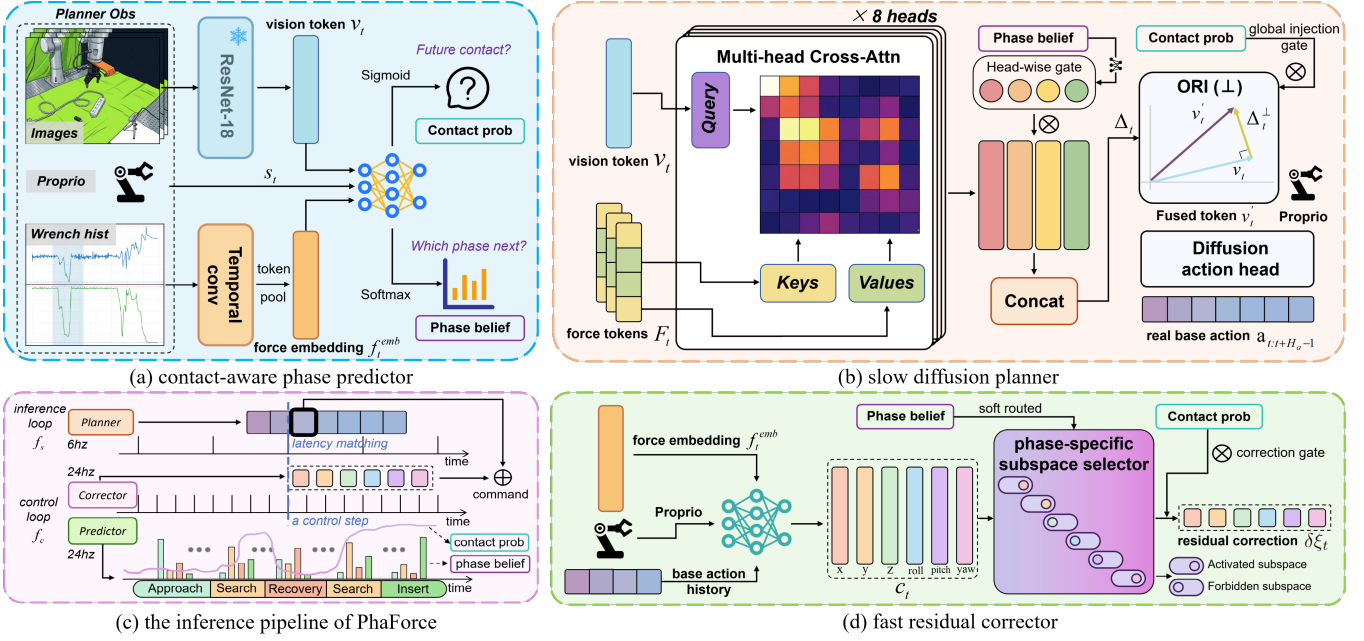


Fig. 2. **PhaForce Architecture.** The **Slow** diffusion planner runs at  $f_s=6$  Hz to generate action chunks, while **CAP** and the **Fast** corrector run at the control rate  $f_c=24$  Hz for contact/phase prediction and within-chunk closed-loop correction. In **Slow**, dual-gated vision–force fusion with orthogonal residual injection preserves vision-dominant task semantics. In **Fast**, phase-belief soft routing activates corrective subspaces and outputs a residual correction that is composed with the Slow base action to obtain the executed command.

correction. The executed pose is composed on  $SE(3)$  as

$$T_t = T_t^{\text{slow}} \circ \Delta T_t^{\text{fast}}. \quad (1)$$

In practice, we represent each pose  $T_t \in SE(3)$  by position and a unit quaternion, and send the low-level command  $a_t \in \mathbb{R}^8$  with gripper width.

### B. Contact-Aware Phase Predictor

Beyond contact state, contact-rich tasks are inherently multi-phase; different phases demand different force usage and corrective subspaces (e.g., planar search vs. normal compliance). To explicitly represent such task progress, for each task we define  $K$  task-specific phases (e.g., *approach/search/recovery/insert/done* in plug-in tasks) and predict a continuous contact probability  $p_t^c \in [0, 1]$  and a phase belief  $\mathbf{p}_t \in \Delta^{K-1}$  (with  $\sum_{k=1}^K \mathbf{p}_t^{(k)} = 1$ ), which are evaluated at  $f_c$  and used to schedule force usage in **Slow** and **Fast** (Secs. III-C–III-D).

**Inputs and outputs.** As shown in Fig. 2(a), we introduce a lightweight predictor **CAP**, denoted as  $\pi_{\text{CAP}}$ , which takes the planner observation  $o_t^p = (\mathcal{I}_t, w_t^{\text{hist}}, s_t)$  as input and outputs  $(p_t^c, \mathbf{p}_t)$ . We use a ResNet-18 for each RGB view without weight sharing to extract visual features, which are fused with force/proprio features by a small MLP, followed by a binary contact head and a categorical phase head.

**Force encoder.** To encode the wrench history  $w_t^{\text{hist}}$  while capturing both abrupt interaction transients and short-term temporal dependencies, we use a lightweight TCN-style temporal encoder shared across **CAP**, **Slow**, and **Fast**. It is implemented as a stack of dilated 1D convolutions with

residual connections, providing multi-scale temporal receptive fields that are sensitive to short-lived F/T changes. For **Slow**, the encoder outputs a sequence of force tokens  $\{f_{t-i}\}_{i=0}^{H_w-1}$  with  $f_{t-i} \in \mathbb{R}^d$ ; for modules that require a single vector (**CAP/Fast**), we additionally apply temporal pooling to obtain a compact force embedding  $f_t^{\text{emb}} \in \mathbb{R}^{d_f}$ .

**Targets and loss.** Importantly,  $\pi_{\text{CAP}}$  is trained for *anticipation* rather than instantaneous judgment. We supervise the contact head using a future-window label indicating whether contact will occur within the next  $K_f$  control steps:  $y_t^c = \bigvee_{i=1}^{K_f} \text{contact}_{t+i}$  and supervise the phase head using a future offset label  $y_t^{\text{phase}} = \text{phase}_{t+\delta}$ . Let  $\ell_t^c \in \mathbb{R}$  and  $\ell_t^\phi \in \mathbb{R}^K$  denote the contact/phase logits, with  $p_t^c = \sigma(\ell_t^c)$  and  $\mathbf{p}_t = \text{softmax}(\ell_t^\phi)$ . We optimize a multi-task objective:

$$\mathcal{L}_{\text{CAP}} = \mathcal{L}_{\text{BCE}}(y_t^c, \ell_t^c) + \lambda_\phi \mathcal{L}_{\text{CE}}(y_t^{\text{phase}}, \ell_t^\phi), \quad (2)$$

where  $\mathcal{L}_{\text{BCE}}$  is binary cross-entropy (with logits) for future contact prediction and  $\mathcal{L}_{\text{CE}}$  is cross-entropy for phase prediction. All labels are automatically generated via scripts using wrench signals and TCP pose, avoiding manual annotation.

### C. Slow Diffusion Planner

As shown in Fig. 2(b), the **Slow** diffusion planner  $\pi_{\text{slow}}$  runs at rate  $f_s$  with an augmented planner input  $\tilde{o}_t^p = (o_t^p, p_t^c, \mathbf{p}_t)$  and outputs an executable action chunk of horizon  $H_a$  in control steps:

$$\mathbf{a}_{t:t+H_a-1} \sim \pi_{\text{slow}}(\cdot | \tilde{o}_t^p). \quad (3)$$

**Encoders.** We encode the multi-view RGB observation into a single visual token  $v_t \in \mathbb{R}^d$  by concatenating per-view global embeddings extracted by ResNet-18 encoders,

and encode the wrench history into force tokens  $F_t \in \mathbb{R}^{H_w \times d}$  using the force encoder described in Sec. III-B.

**Dual-gated fusion.** We fuse vision and force via a multi-head cross-attention block, which uses the visual token as a query to attentively aggregate the force tokens.

Let  $Q = v_t W_Q \in \mathbb{R}^{1 \times d_k}$  and  $K = F_t W_K$ ,  $V = F_t W_V \in \mathbb{R}^{H_w \times d_k}$  where  $W_Q, W_K, W_V \in \mathbb{R}^{d \times d_k}$ . For a single head,

$$\text{Attn}(Q, K, V) = \text{softmax}\left(\frac{QK^\top}{\sqrt{d_k}}\right)V. \quad (4)$$

To make force usage phase-dependent and interpretable, we introduce a phase-dependent *head-wise gate*

$$g_t^{\text{head}} = \sigma(\text{MLP}(\mathbf{p}_t)) \in [0, 1]^H, \quad (5)$$

where  $g_t^{\text{head}}(h)$  denotes its  $h$ -th element. We reweight per-head outputs by  $g_t^{\text{head}}$  and obtain the cross-attention output

$$\Delta_t = W_O [g_t^{\text{head}}(1) \text{Attn}_1; \dots; g_t^{\text{head}}(H) \text{Attn}_H], \quad (6)$$

where  $\text{Attn}_h$  denotes the output of head  $h$  computed by Eq. (4) with head-specific projections, and  $W_O$  is the output projection. In addition, a *global injection gate*  $g_t^c = p_t^c$  controls the injection strength in Eq. (8), suppressing the influence of noisy wrench signals in free-space.

**Orthogonal residual injection (ORI).** Rather than overwriting the visual feature with  $\Delta_t$ , we inject it as a *residual* and retain only its component *orthogonal* to the visual token, preserving vision-dominant semantics and mitigating semantic drift.

$$\Delta_t^\perp = \Delta_t - \text{Proj}_{v_t}(\Delta_t) = \Delta_t - \frac{\langle \Delta_t, v_t \rangle}{\langle v_t, v_t \rangle + \epsilon} v_t, \quad (7)$$

where  $\epsilon = 10^{-6}$  is a numerical stabilizer. The fused token is then

$$v_t' = v_t + \alpha \cdot g_t^c \cdot \Delta_t^\perp, \quad (8)$$

where  $\alpha$  is a learnable scalar gain that is clipped to a bounded range for stability. Intuitively,  $p_t^c$  controls *when / how much* force should influence planning, while  $\mathbf{p}_t$  controls *which heads* are emphasized under the current phase.

**Diffusion-based chunk planning.** Given the conditioning  $z_t = \text{cond}(v_t', s_t)$ , we use a diffusion action head to generate an action chunk by progressively denoising a noisy action trajectory into executable commands [1], [29], [30]. In training, the rotational component is represented by 6DRot.

#### D. Fast Residual Corrector

As shown in Fig. 2(d), the **Fast** corrector  $\pi_{\text{fast}}$  runs at rate  $f_c$  with an augmented corrector input  $\tilde{o}_t^c = (o_t^c, \mathbf{h}_t^{\text{slow}}, p_t^c, \mathbf{p}_t)$ , where  $\mathbf{h}_t^{\text{slow}}$  denotes a short history of base actions produced by **Slow**. **Fast** predicts an intermediate within-chunk *channel-wise* residual  $c_t$ :

$$c_t = \pi_{\text{fast}}(\tilde{o}_t^c) \in \mathbb{R}^6, \quad (9)$$

where  $c_t = [c_x, c_y, c_z, c_{\text{roll}}, c_{\text{pitch}}, c_{\text{yaw}}]^\top$ .

**Phase-routed corrective subspaces.** The channel residual  $c_t$  specifies residual increments along interpretable correction

channels. For each phase  $k \in \{1, \dots, K\}$ , we predefine a *phase-specific subspace selector*  $B_k \in \mathbb{R}^{6 \times 6}$  as a diagonal binary channel mask, i.e.,  $B_k = \text{diag}(m_k)$  with  $m_k \in \{0, 1\}^6$ , which disables *forbidden* dimensions and keeps only the *activated* channels in that phase. For example, in plug-in tasks, the *search* phase activates  $(x, y, \text{yaw})$  (e.g.,  $m_{\text{search}} = [1, 1, 0, 0, 0, 1]$ ), whereas the *insert* phase activates normal compliance along  $(z, \text{yaw})$ . We then obtain the residual twist by *softly routing* the raw channel-wise residual  $c_t$  using the phase belief, with contact gating by  $p_t^c$ :

$$\delta \xi_t = p_t^c \left( \sum_{k=1}^K \mathbf{p}_t^{(k)} B_k \right) c_t \in \mathbb{R}^6, \quad (10)$$

For execution,  $\delta \xi_t$  is converted to the pose increment  $\Delta T_t^{\text{fast}}$ . Unlike admittance controllers that typically rely on fixed gains and hand-designed DOF switching, phase-belief soft routing smoothly interpolates among phase-specific corrective subspaces. Moreover, contact gating suppresses spurious corrections induced by free-space wrench noise without additional heuristic thresholds or filtering.

**Physical-prior supervision.** In contact-rich tasks, beyond the nominal TCP pose, we consider a *virtual target pose* that the robot would track under compliant interaction, as implied by force feedback [14]. Rather than explicitly estimating this target pose, we treat the desired *pose offset* as a residual twist and specify it via a phase-dependent physical prior, yielding automatic supervision for **Fast**. Concretely, we construct phase-wise physically motivated residual targets  $\delta \xi_{t,k}^* \in \mathbb{R}^6$  from wrench signals to capture desired corrective trends in each phase. For example, during planar *search*, the target drives the robot to relieve tangential friction and mitigate jamming torques:

$$\delta \xi_{t,\text{search}}^* = [-\alpha_x F_{x,t}, -\alpha_y F_{y,t}, 0, 0, 0, -\alpha_{\text{yaw}} \tau_{z,t}]^\top, \quad (11)$$

where we treat roll/pitch as a *forbidden subspace* to promote stable execution. During *wiping*, the target enforces normal compliance by tracking a desired normal force  $F_z^*$ :

$$\delta \xi_{t,\text{wiping}}^* = [0, 0, \alpha_z (F_z^* - F_{z,t}), 0, 0, 0]^\top. \quad (12)$$

Similar targets can be defined for rotation channels using measured torques. To keep supervision consistent with the soft-routed correction in Eq. (10), we compute a single target by phase-belief-weighted averaging of phase-wise residual priors, with correction gating by  $p_t^c$ :

$$\delta \xi_t^* = p_t^c \sum_{k=1}^K \mathbf{p}_t^{(k)} \delta \xi_{t,k}^*. \quad (13)$$

**Training loss.** We regress  $\delta \xi_t$  to  $\delta \xi_t^*$  with an  $\ell_1$  loss:

$$\mathcal{L}_{\text{fast}} = \mathbb{E} [\|\delta \xi_t - \delta \xi_t^*\|_1]. \quad (14)$$

## IV. EXPERIMENTS

### A. Experimental Setup

Our experiments are conducted on a Flexiv Rizon 4s robotic arm equipped with a 6-axis force/torque sensor

at the end effector. We use one wrist-mounted and two external Intel RealSense D435 cameras to provide multi-view RGB observations. We collect 80 expert teleoperated demonstrations per task using TactAR [18], which provides real-time *wrench visualization* to refine contact behaviors. All devices are connected to a workstation with an Intel Core i7-14700F CPU and an NVIDIA RTX 4060 Ti GPU for data collection and policy evaluation.

### B. Tasks and Metrics

**Tasks.** We evaluate PhaForce on five real-robot contact-rich tasks with task-defined phases for **CAP**, capturing phase-dependent corrective subspaces beyond normal-force compliance (e.g., tangential friction and torque cues for planar alignment and jamming relief). Table I summarizes the phase-specific activated subspaces for **Fast**.

**(i) Charger Plug-in.** Phases:  $\{approach, search, recovery, insert, done\}$ . *Search* performs planar hole-alignment, where tangential friction forces and torques reveal misalignment and hole rim contact; thus corrections mainly lie in a planar subspace. *Recovery* indicates severe sticking or large wrench transients and requires an explicit retreat-and-retry intent switch, handled by the **Slow** planner rather than within-phase **Fast** micro-correction. Notably, *Recovery* may not occur in every episode; it is activated only when the above conditions are detected, while many successful trials proceed with *search* followed by *insert*. *Insert* emphasizes continuous advancement toward a fully seated insertion.

**(ii) USB Plug-in.** Phases: same as (i). In our setup, USB is more sensitive to small planar/yaw misalignment, often exhibiting friction-induced stick-slip and transient torques due to edge contact under tight tolerances.

**(iii) Drawer Opening.** Phases:  $\{pick, unlock, pull, done\}$ . *Unlock* overcomes initial stiction. *Pull* follows the drawer’s constraint-guided sliding motion, where wrench feedback enforces directional compliance—driving along the opening direction while suppressing lateral forces that cause binding.

**(iv) Wiping (ID).** Phases:  $\{pick, approach, wiping, done\}$ . Only *wiping* is force-critical: vision is ambiguous about contact quality, as slight detachment yields ineffective wiping while over-pressing increases friction and induces oscillation; thus normal force feedback provides a direct signal for maintaining effective contact.

**(v) Wiping (OOD).** Same phases as ID, but the board is raised by 3 cm at test time while demonstrations are collected at the original height, creating an out-of-distribution contact condition. This further tests whether a policy can leverage force feedback to compensate for unseen contact geometry and maintain stable wiping.

**Metrics.** For each method and each task, we run 20 evaluation trials with randomized initial conditions and report the success rate (SR). For plug-in tasks, we regard partial insertion that does not reach a fully seated state as failure. For wiping, we additionally evaluate contact quality and wiping effectiveness in Sec. IV-E.

TABLE I

CORRECTIVE SUBSPACES FOR FORCE-CRITICAL PHASES ACROSS TASKS

subspace	search	insert	unlock	pull	wiping
$x$	✓		✓	✓	
$y$	✓		✓	✓	
$z$		✓			✓
roll				✓	
pitch				✓	
yaw	✓	✓			

TABLE II

SUCCESS RATE (SR, %) ACROSS DIFFERENT POLICIES.

Method	Charger	USB	Drawer	Wipe-ID	Wipe-OOD	Avg
DP	20	15	60	<b>95</b>	0	38
DP (force-concat)	20	20	50	85	0	35
RDP	50	55	65	85	75	66
PhaForce (ours)	<b>80</b>	<b>85</b>	<b>85</b>	<b>95</b>	<b>85</b>	<b>86</b>

### C. Baselines and Implementation

**Baselines.** We compare against four methods: (i) *Diffusion Policy (DP)* [1], a strong vision-only imitation learning policy; (ii) *DP (force-concat)*, which directly concatenates the force feature with the vision feature for action generation; (iii) *RDP* [18], a representative slow-fast diffusion policy that leverages high-rate wrench/tactile feedback for within-chunk reactive execution; and (iv) *PhaForce (Ours)*.

**Implementation.** For all methods, diffusion runs at  $f_s = 6$  Hz and we execute at a control rate of  $f_c = 24$  Hz with an action-chunk horizon  $H_a = 16$ ; we adopt latency matching by discarding the first few steps following UMI [31] and RDP [18], and send interpolated actions to the low-level controller at  $> 500$  Hz. For *PhaForce*, we use a wrench-history window of  $H_w = 36$  ( $\approx 1.5$  s) to capture short-term interaction dynamics. Each RGB view is encoded into a 512-d embedding and concatenated into a visual token of dimension  $d = 1536$ . For **CAP**, we set  $\delta = 3$ ,  $K_f = 8$ , and  $\lambda_\phi = 2$ . In **Slow**, we use multi-head cross-attention with  $H = 8$  heads (per-head dimension  $d_k = d/H = 192$ ). For diffusion, we use a DDIM scheduler with  $\epsilon$ -prediction, using 100 timesteps at training and 10 timesteps at inference. For the physical-prior teachers in **Fast**, we set  $\alpha_x = \alpha_y = \alpha_z = 5 \times 10^{-5}$  m/N and  $\alpha_{\text{roll}} = \alpha_{\text{pitch}} = \alpha_{\text{yaw}} = 3 \times 10^{-2}$  rad/(N · m). The average inference time per run is  $\sim 120$  ms (Slow),  $\sim 3$  ms (CAP), and  $< 1$  ms (Fast).

### D. Results and Analysis

Table II reports success rates across five real-robot tasks. Overall, **PhaForce** achieves the best (or tied-best) performance on all tasks. Averaged over the three baselines, **PhaForce** improves the mean SR by **+40** pp. Fig. 3 further shows **PhaForce**’s execution over time, highlighting phase switches throughout each task.

**Plug-in tasks.** Insertion is highly sensitive to small pose errors and local contact geometry, and typically involves phase switches such as planar search and recovery. As

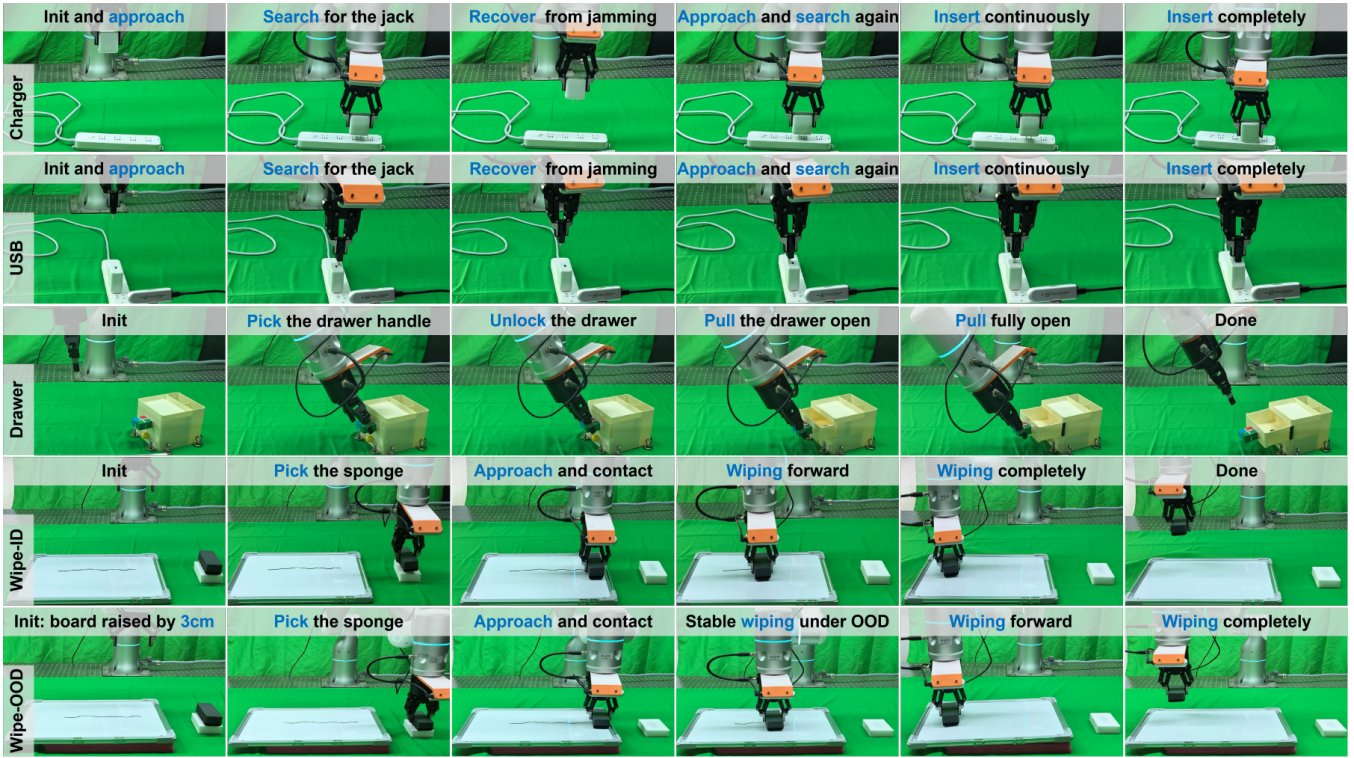


Fig. 3. We design five contact-rich tasks; each task exhibits *varying contact states and phase belief*, and each phase activates different corrective subspaces. Each row illustrates the phase transitions in a task. PhaForce not only excels on in-distribution tasks but also remains stable under OOD shifts.

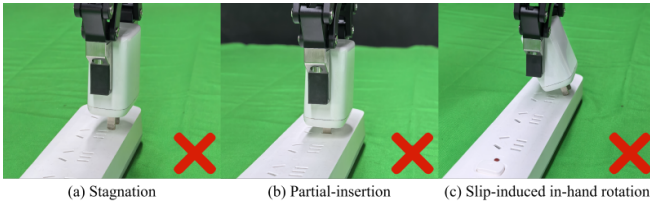


Fig. 4. Three common baseline failure modes in plug-in tasks.

shown in Fig. 4, we observe three common failure modes of baselines: (i) *Stagnation*: after a slight misalignment, the end-effector gets stuck at the socket entrance and fails to trigger planar search or retreat-and-retry. (ii) *Partial insertion*: the plug enters the socket but remains not fully seated, resulting in an incomplete insertion. (iii) *Slip-induced in-hand rotation*: rim collisions with excessive contact force can cause the connector to slip inside the gripper and rotate substantially, misorienting the plug. The last mode is an *unintended* disturbance rather than an intended search subspace, and is difficult to compensate without demonstrations covering large reorientation.

*DP* often fails to achieve millimeter-level alignment because it must infer the contact state and corrective direction purely from images. *DP (force-concat)* yields only limited gains because naive wrench concatenation lacks an explicit mechanism to convert high-frequency force feedback into timely within-chunk micro-corrections [18].

*RDP* improves performance via fast closed-loop refine-

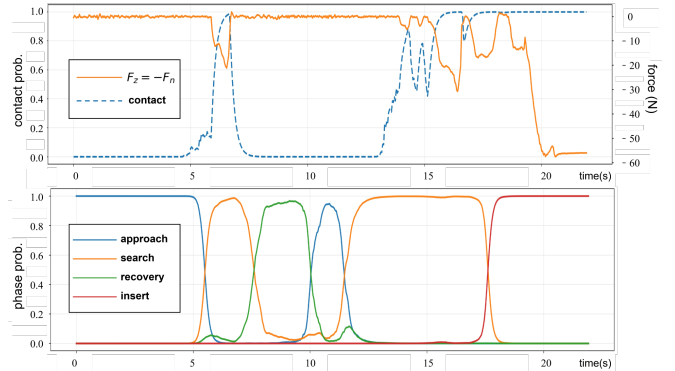


Fig. 5. We visualize the contact probability, phase belief, and  $z$ -axis force  $F_z$  in a USB Plug-in task (curves are smoothed for visualization).

ment, yet it still underperforms **PhaForce** on fine insertion. We conjecture that, for such millimeter-sensitive tasks, latent action-space planning can degrade execution precision for contact alignment, consistent with the precision-loss effects attributed to latent compression in [28]. In contrast, **PhaForce's Slow** predicts executable actions directly in the *real* action space, rather than latent space. Moreover, without an explicit phase belief, RDP may struggle to reliably switch into *recovery*, making it harder to escape stagnation at the socket entrance.

**PhaForce** mitigates these issues by using phase belief to condition and gate search/recovery behaviors, enabling timely retreat-and-retry instead of stagnation. As shown in

TABLE III  
WIPING (ID): DEEPER EVALUATION BEYOND SR.

Method	SR	Score	$\overline{F}_n$ (N)	Over	Under
DP	<b>95</b>	0.80	17.3	21.5%	7.4%
DP (force-concat)	85	0.75	17.0	16.8%	5.6%
RDP	85	0.65	13.6	5.7%	2.3%
PhaForce w/o Fast	<b>95</b>	0.70	15.1	14.3%	5.0%
PhaForce (ours)	<b>95</b>	<b>0.85</b>	12.3	<b>4.5%</b>	<b>2.0%</b>

TABLE IV  
WIPING (OOD): DEEPER EVALUATION BEYOND SR (- DENOTES A METRIC THAT IS NOT APPLICABLE WHEN SR=0).

Method	SR	Score	$\overline{F}_n$ (N)	Over	Under
DP	0	-	46.2	85.3%	-
DP (force-concat)	0	-	44.6	86.7%	-
RDP	75	0.65	9.2	7.2%	<b>0.22%</b>
PhaForce w/o Fast	0	-	48.3	80.3%	-
PhaForce (ours)	<b>85</b>	<b>0.75</b>	14.3	<b>7.0%</b>	0.34%

Fig. 5, CAP’s anticipatory contact/phase predictions align with wrench transients. Moreover, **PhaForce** applies targeted within-chunk residual corrections in task-relevant subspaces while preserving the vision-conditioned semantics of the slow planning chunk. It also alleviates partial-insertion failures where baselines engage the hole yet fail to achieve a fully seated insertion. For slip events, we reduce their occurrence by avoiding excessive contact and by triggering recovery once abnormal wrench signals are detected; handling large in-hand rotations more fundamentally remains future work (e.g., explicit in-hand pose estimation or enriched demonstrations).

**Drawer task.** For Drawer Opening, **PhaForce** achieves a consistent improvement and we attribute this gain to phase-aware force utilization that facilitates compliant pulling (with small roll/pitch compliance) under friction variations and occasional binding, enabling timely adjustments rather than persisting with a misaligned pull.

#### E. Wiping: Contact Quality and Effectiveness

Success rate alone is insufficient for wiping, since a policy may complete the motion while applying excessive force or experiencing frequent contact dropouts. For both ID and OOD, we report a wiping score (1 for fully wiped, 0.5 for partial wiping, and 0 for no erasure), mean contact normal force  $\overline{F}_n$ , and the over-pressure ( $F_n > 25$  N) / under-pressure ( $F_n < 2.5$  N) time ratios. For reference, in our demonstrations the mean normal force during contact is 18.7 N; we empirically set the target normal force to  $F_n^* = 12$  N, corresponding to  $F_z^* = -12$  N under the convention  $F_z = -F_n$ , to reduce over-pressure while maintaining reliable erasure.

**Wiping (ID).** As shown in Table III, **PhaForce** achieves the best overall wiping outcome, with the highest score, the lowest under-/over-pressure ratios. By contrast, *DP* attains strong SR/Score, but its contact quality is unstable, with

TABLE V  
ABLATION RESULTS OVER 20 REAL-ROBOT TRIALS PER METHOD.

Method	USB SR	Wipe-OOD SR	Wiping Score
PhaForce (w/o PB)	25	45	0.60
PhaForce (w/o ORI)	35	60	0.45
PhaForce (w/o Fast)	50	0	-
PhaForce (ours)	<b>85</b>	<b>85</b>	<b>0.75</b>

frequent over-pressure and contact dropouts, consistent with small teleoperation jitter in demonstrations manifesting as force fluctuations during contact. *DP (force-concat)* and *RDP* occasionally fail to grasp the sponge, highlighting the risk of using wrench feedback without phase scheduling: in non-contact stages, wrench signals are often noise-dominated, thereby hurting overall performance [19]. Meanwhile, *RDP* markedly reduces unstable contact events, yet yields a lower wiping score, plausibly because latent action-space planning can degrade fine-grained visual localization needed for precise erasing of the notes. Overall, **PhaForce** benefits from (i) **CAP** for unified phase-aware scheduling of force usage, (ii) **Slow** visual-force fusion via *ORI* that preserves vision-dominant task semantics, and (iii) the **Fast** corrector regulates the contact normal force via force feedback in the corrective subspace.

**Wiping (OOD).** As shown in Table IV, chunk-level diffusion planners without fast correction fail completely (*DP*, *DP (force-concat)*, and *PhaForce w/o Fast*), exhibiting sustained over-pressure and zero success. This collapse is mainly due to the height mismatch: the policy overfits to the demonstration height, causing the end-effector to either over-press and stall or stick to the board and drag quasi-statically under large friction, thus failing to execute the intended wiping motion. In contrast, *RDP* remains feasible under OOD, highlighting the advantage of a slow-fast design for contact adaptation, and **PhaForce** further improves wiping score with comparable contact stability, showing that **Fast** is key to compensating the OOD height mismatch.

#### F. Ablations

To validate the effectiveness of key components of **PhaForce**, we conduct ablations on two representative tasks: *USB Plug-in*, a multi-phase task with distinct phase transitions, and *Wiping (OOD)*, which requires robust contact adaptation under environment shifts. Specifically, we consider three ablation variants: (i) *PhaForce (w/o PB)*, removing phase belief by replacing  $\mathbf{p}_t$  with a uniform prior over  $K$  phases during both training and testing, i.e.,  $p_t^{(k)} \equiv 1/K$ ; (ii) *PhaForce (w/o ORI)*, replacing the fused token  $v'_t$  with the cross-attention output  $\Delta_t$  as diffusion conditioning; and (iii) *PhaForce (w/o Fast)*, removing the **Fast** residual corrector.

**Results.** Table V shows that removing phase belief (*w/o PB*) severely hurts *USB Plug-in* (SR 85→25), indicating that explicit phase scheduling is essential to *route* corrections to the right subspaces and *trigger* timely search/recovery/insert transitions in a multi-phase insertion. Replacing *ORI* with direct cross-attention conditioning (*w/o ORI*) degrades both

SR and wiping score on *Wipe-OOD* (SR 85→60; score 0.75→0.45), supporting that *ORI* preserves vision-dominant semantics while injecting force information. Finally, removing **Fast** (*w/o Fast*) collapses *Wipe-OOD* (SR 0), confirming that high-rate residual correction is indispensable for stabilizing contact (rapidly compensating F/T transients) when the environment deviates from the demonstrations.

## V. CONCLUSIONS

In this paper, we propose **PhaForce**, a phase-scheduled visual–force policy learning framework that integrates low-rate generative planning with high-rate reactive correction for contact-rich manipulation. PhaForce combines a contact-aware phase predictor (**CAP**) that delivers a global contact/phase schedule, a **Slow** diffusion planner that performs dual-gated vision–force fusion with orthogonal residual injection, and a **Fast** residual corrector that performs within-chunk, subspace-specific closed-loop refinement. Real-robot experiments across five tasks show that PhaForce consistently outperforms strong baselines in both ID and OOD settings, excelling in both phase-transition-intensive skills and sustained-contact skills beyond success rate alone. Future work will explore learning the Fast corrector with reinforcement learning beyond supervised residual targets, and extend PhaForce from single-task imitation to VLA models that generalize across diverse skills and embodiments.

## REFERENCES

- [1] C. Chi, Z. Xu, S. Feng, E. Cousineau, Y. Du, B. Burchfiel, R. Tedrake, and S. Song, “Diffusion policy: Visuomotor policy learning via action diffusion,” *The International Journal of Robotics Research*, vol. 44, no. 10-11, pp. 1684–1704, 2025.
- [2] M. J. Kim, K. Pertsch, S. Karamcheti, T. Xiao, A. Balakrishna, S. Nair, R. Rafailov, E. Foster, G. Lam, P. Sanketi *et al.*, “Open-vla: An open-source vision-language-action model,” *arXiv preprint arXiv:2406.09246*, 2024.
- [3] K. Black, N. Brown, D. Driess, A. Esmail, M. Equi, C. Finn, N. Fusai, L. Groom, K. Hausman, B. Ichter *et al.*, “ $\pi_0$ : A Vision-Language-Action Flow Model for General Robot Control,” *arXiv preprint arXiv:2410.24164*, 2024.
- [4] Physical Intelligence, K. Black, N. Brown, J. Darpinian, K. Dhabalia, D. Driess, A. Esmail, M. Equi, C. Finn, N. Fusai *et al.*, “ $\pi_{0.5}$ : A Vision-Language-Action Model with Open-World Generalization,” *arXiv preprint arXiv:2504.16054*, 2025.
- [5] T. Z. Zhao, V. Kumar, S. Levine, and C. Finn, “Learning fine-grained bimanual manipulation with low-cost hardware,” *arXiv preprint arXiv:2304.13705*, 2023.
- [6] S. Liu, L. Wu, B. Li, H. Tan, H. Chen, Z. Wang, K. Xu, H. Su, and J. Zhu, “Rdt-1b: a diffusion foundation model for bimanual manipulation,” *arXiv preprint arXiv:2410.07864*, 2024.
- [7] Z. Sun, Y. Wang, D. Held, and Z. Erickson, “Force-constrained visual policy: Safe robot-assisted dressing via multi-modal sensing,” *IEEE Robotics and Automation Letters*, vol. 9, no. 5, pp. 4178–4185, 2024.
- [8] S. Stepputtis, M. Bandari, S. Schaal, and H. B. Amor, “A system for imitation learning of contact-rich bimanual manipulation policies,” in *2022 IEEE/RSJ International Conference on Intelligent Robots and Systems (IROS)*. IEEE, 2022, pp. 11 810–11 817.
- [9] X. Zhang, C. Zhang, B. Zhang, Z. Peng, S. Cui, and S. Wang, “Dextac: Learning contact-aware visuotactile policies via hand-by-hand teaching,” *arXiv preprint arXiv:2601.21474*, 2026.
- [10] Y. Wu, Z. Chen, F. Wu, L. Chen, L. Zhang, Z. Bing, A. Swikir, S. Haddadin, and A. Knoll, “Tacdiffusion: Force-domain diffusion policy for precise tactile manipulation,” in *2025 IEEE International Conference on Robotics and Automation (ICRA)*. IEEE, 2025, pp. 11 831–11 837.
- [11] C. Tsuji, E. Coronado, P. Osorio, and G. Venture, “Adaptive contact-rich manipulation through few-shot imitation learning with force-torque feedback and pre-trained object representations,” *IEEE Robotics and Automation Letters*, vol. 10, no. 1, pp. 240–247, 2024.
- [12] C. Chen, Z. Yu, H. Choi, M. Cutkosky, and J. Bohg, “Dexforce: Extracting force-informed actions from kinesthetic demonstrations for dexterous manipulation,” *IEEE Robotics and Automation Letters*, 2025.
- [13] Z. Zhang, H. Xu, Z. Yang, C. Yue, Z. Lin, H.-a. Gao, Z. Wang, and H. Zhao, “Ta-vla: Elucidating the design space of torque-aware vision-language-action models,” *arXiv preprint arXiv:2509.07962*, 2025.
- [14] Y. Hou, Z. Liu, C. Chi, E. Cousineau, N. Kuppuswamy, S. Feng, B. Burchfiel, and S. Song, “Adaptive compliance policy: Learning approximate compliance for diffusion guided control,” in *2025 IEEE International Conference on Robotics and Automation (ICRA)*. IEEE, 2025, pp. 4829–4836.
- [15] J. Li, T. Wu, J. Zhang, Z. Chen, H. Jin, M. Wu, Y. Shen, Y. Yang, and H. Dong, “Adaptive visuo-tactile fusion with predictive force attention for dexterous manipulation,” in *2025 IEEE/RSJ International Conference on Intelligent Robots and Systems (IROS)*. IEEE, 2025, pp. 3232–3239.
- [16] J. Yu, H. Liu, Q. Yu, J. Ren, C. Hao, H. Ding, G. Huang, G. Huang, Y. Song, P. Cai *et al.*, “Forcevla: Enhancing vla models with a force-aware moe for contact-rich manipulation,” *arXiv preprint arXiv:2505.22159*, 2025.
- [17] B. Zhou, R. Jiao, Y. Li, X. Yuan, F. Fang, and S. Li, “Admittance visuomotor policy learning for general-purpose contact-rich manipulations,” *IEEE Transactions on Industrial Electronics*, 2025.
- [18] H. Xue, J. Ren, W. Chen, G. Zhang, Y. Fang, G. Gu, H. Xu, and C. Lu, “Reactive diffusion policy: Slow-fast visual-tactile policy learning for contact-rich manipulation,” *arXiv preprint arXiv:2503.02881*, 2025.
- [19] Z. He, H. Fang, J. Chen, H.-S. Fang, and C. Lu, “Foar: Force-aware reactive policy for contact-rich robotic manipulation,” *IEEE Robotics and Automation Letters*, 2025.
- [20] G. Lee, Y. Lee, K. Kim, S. Lee, S. Noh, S. Back, and K. Lee, “Manipforce: Force-guided policy learning with frequency-aware representation for contact-rich manipulation,” *arXiv preprint arXiv:2509.19047*, 2025.
- [21] T. Li, Y. Li, Z. Zhang, and N. Figueroa, “Flow with the force field: Learning 3d compliant flow matching policies from force and demonstration-guided simulation data,” *arXiv preprint arXiv:2510.02738*, 2025.
- [22] W. Liu, J. Wang, Y. Wang, W. Wang, and C. Lu, “Forcemimic: Force-centric imitation learning with force-motion capture system for contact-rich manipulation,” in *2025 IEEE International Conference on Robotics and Automation (ICRA)*. IEEE, 2025, pp. 1105–1112.
- [23] H. Ge, Y. Jia, Z. Li, Y. Li, Z. Chen, R. Huang, and G. Zhou, “Filic: Dual-loop force-guided imitation learning with impedance torque control for contact-rich manipulation tasks,” *arXiv preprint arXiv:2509.17053*, 2025.
- [24] H. Choi, Y. Hou, C. Pan, S. Hong, A. Patel, X. Xu, M. R. Cutkosky, and S. Song, “In-the-wild compliant manipulation with umi-ft,” *arXiv preprint arXiv:2601.09988*, 2026.
- [25] M. Aburub, C. C. Beltran-Hernandez, T. Kamijo, and M. Hamaya, “Learning diffusion policies from demonstrations for compliant contact-rich manipulation,” *arXiv preprint arXiv:2410.19235*, 2024.
- [26] T. Kamijo, C. C. Beltran-Hernandez, and M. Hamaya, “Learning variable compliance control from a few demonstrations for bimanual robot with haptic feedback teleoperation system,” in *2024 IEEE/RSJ International Conference on Intelligent Robots and Systems (IROS)*. IEEE, 2024, pp. 12 663–12 670.
- [27] J. H. Kang, S. Joshi, R. Huang, and S. K. Gupta, “Robotic compliant object prying using diffusion policy guided by vision and force observations,” *IEEE Robotics and Automation Letters*, 2025.
- [28] W. Chen, H. Xue, Y. Wang, F. Zhou, J. Lv, Y. Jin, S. Tang, C. Wen, and C. Lu, “Implicitrdp: An end-to-end visual-force diffusion policy with structural slow-fast learning,” *arXiv preprint arXiv:2512.10946*, 2025.
- [29] J. Ho, A. Jain, and P. Abbeel, “Denosing diffusion probabilistic models,” *Advances in neural information processing systems*, vol. 33, pp. 6840–6851, 2020.
- [30] J. Song, C. Meng, and S. Ermon, “Denosing diffusion implicit models,” *arXiv preprint arXiv:2010.02502*, 2020.
- [31] C. Chi, Z. Xu, C. Pan, E. Cousineau, B. Burchfiel, S. Feng, R. Tedrake, and S. Song, “Universal manipulation interface: In-the-wild robot

teaching without in-the-wild robots," *arXiv preprint arXiv:2402.10329*, 2024.